

# Geophysical Research Letters<sup>®</sup>



## RESEARCH LETTER

10.1029/2022GL102383

### Key Points:

- Hydrogen trapping and rearrangement in porous rock have been observed in situ
- Ostwald ripening is observed over timescales consistent with theoretical predictions
- The results imply less trapping and hysteresis than with completely insoluble gas

### Correspondence to:

Y. Zhang and M. J. Blunt,  
yihuai.zhang@glasgow.ac.uk;  
m.blunt@imperial.ac.uk

### Citation:

Zhang, Y., Bijeljic, B., Gao, Y., Goodarzi, S., Foroughi, S., & Blunt, M. J. (2023). Pore-scale observations of hydrogen trapping and migration in porous rock: Demonstrating the effect of Ostwald ripening. *Geophysical Research Letters*, 50, e2022GL102383. <https://doi.org/10.1029/2022GL102383>

Received 5 DEC 2022  
Accepted 11 MAR 2023





### Author Contributions:

**Conceptualization:** Yihuai Zhang, Ying Gao, Sepideh Goodarzi, Martin J. Blunt  
**Data curation:** Yihuai Zhang, Ying Gao  
**Formal analysis:** Yihuai Zhang, Sajjad Foroughi, Martin J. Blunt  
**Funding acquisition:** Branko Bijeljic, Martin J. Blunt  
**Investigation:** Yihuai Zhang, Branko Bijeljic, Ying Gao, Sajjad Foroughi, Martin J. Blunt  
**Methodology:** Yihuai Zhang, Branko Bijeljic, Sepideh Goodarzi, Sajjad Foroughi, Martin J. Blunt  
**Project Administration:** Branko Bijeljic, Martin J. Blunt  
**Resources:** Yihuai Zhang, Branko Bijeljic, Sepideh Goodarzi  
**Software:** Yihuai Zhang, Sajjad Foroughi  
**Supervision:** Branko Bijeljic, Martin J. Blunt

© 2023 The Authors.

This is an open access article under the terms of the [Creative Commons Attribution-NonCommercial License](https://creativecommons.org/licenses/by/4.0/), which permits use, distribution and reproduction in any medium, provided the original work is properly cited and is not used for commercial purposes.

## Pore-Scale Observations of Hydrogen Trapping and Migration in Porous Rock: Demonstrating the Effect of Ostwald Ripening

Yihuai Zhang<sup>1,2</sup> , Branko Bijeljic<sup>2</sup> , Ying Gao<sup>3</sup>, Sepideh Goodarzi<sup>2</sup>, Sajjad Foroughi<sup>2</sup> , and Martin J. Blunt<sup>2</sup> 

<sup>1</sup>James Watt School of Engineering, University of Glasgow, Glasgow, UK, <sup>2</sup>Department of Earth Science and Engineering, Imperial College London, London, UK, <sup>3</sup>Shell Global Solutions International B.V., Amsterdam, The Netherlands

**Abstract** We use high-resolution three-dimensional X-ray imaging to study hydrogen injection and withdrawal in the pore space of Bentheimer sandstone. The results are compared with a replicate experiment using nitrogen. We observe less trapping with hydrogen because the initial saturation after drainage is lower due to channeling. Remarkably we observe that after imbibition, if the sample is imaged again after 12 hr, there is a significant rearrangement of the trapped hydrogen. Many smaller ganglia disappear while the larger ganglia swell, with no detectable change in overall gas volume. For nitrogen, the fluid configuration is largely unchanged. This rearrangement is facilitated by concentration gradients of dissolved gas in the aqueous phase—Ostwald ripening. We estimate the time-scales for this effect to be significant, consistent with the experimental observations. The swelling of larger ganglia potentially increases the gas connectivity, leading to less hysteresis and more efficient withdrawal.

**Plain Language Summary** The supply of energy by hydrogen is a key component of a zero-carbon economy; an essential part of global hydrogen use is underground storage at the gigatonne scale in porous rocks. However, the behavior of hydrogen in the subsurface is not well understood. Using high-resolution three-dimensional X-ray imaging, we observe that in the pore-space, there is a significant rearrangement of hydrogen trapped by water. Many smaller trapped bubbles disappear while the larger ones grow. The process is driven by differences in the amount of gas dissolved in the aqueous phase: this is called Ostwald ripening. We estimate the time-scales effect as being important, which are consistent with the experimental observations. The work implies that there is less trapping for hydrogen injection and withdrawal compared to equivalent hydrocarbon systems, which makes the process efficient.

## 1. Introduction

The use of hydrogen as an energy source is widely considered to be a key component of a zero-carbon energy economy (Heinemann et al., 2021; Miocic et al., 2022; Parnell & Blamey, 2017; Zeng et al., 2022). Hydrogen has a high specific energy capacity (120 MJ/kg), larger on a mass basis than natural gas (methane), which makes it a promising replacement for many fossil-fuel-powered applications. However, the hydrogen needs to be stored until needed, particularly bearing in mind the intermittent nature of renewable power generation. At the scale required, running to several Gt ( $10^{12}$  kg) at a global scale, underground storage in depleted hydrocarbon reservoirs, saline aquifers or salt caverns is required (Aftab et al., 2022; Ali et al., 2021; Boon & Hajibeygi, 2022; Hematpur et al., 2023; Muhammed et al., 2022; Raad et al., 2022).

Hydrogen has an extremely low density, low viscosity and high diffusivity, very different from other gases commonly stored or encountered in the subsurface, such as nitrogen, methane, ethane and carbon dioxide. The other challenge is that unlike the one-way nature of most storage or extraction—for instance, with carbon dioxide, we only need to design injection such that the carbon dioxide remains underground—in hydrogen storage, we need to both inject and produce the gas with as little loss of material, or use of energy, as possible.

Contact angle controls the amount of trapping in the pore space: lower contact angles (water-wet conditions) imply more trapping of hydrogen by water leading to less efficient withdrawal (Hashemi et al., 2021; Yekta et al., 2018). Iglauer et al. (2021) found that the contact angle between water and hydrogen on a quartz substrate increases, indicating less water-wet conditions, with pressure and depth. The system became intermediate-wet in the presence of organic material.

**Validation:** Yihuai Zhang, Branko Bijeljic, Ying Gao, Sepideh Goodarzi, Martin J. Blunt  
**Visualization:** Yihuai Zhang, Ying Gao, Sajjad Foroughi  
**Writing – original draft:** Yihuai Zhang  
**Writing – review & editing:** Yihuai Zhang, Ying Gao, Sepideh Goodarzi, Martin J. Blunt

To assess the behavior of hydrogen reliably in representative porous formations, it is necessary to observe in situ the pore-space configurations of the fluids. In recent studies, non-destructive high-resolution three-dimensional X-ray imaging has been used to observe trapped hydrogen inside rock otherwise saturated with an aqueous phase (Jangda et al., 2023; Jha et al., 2021; Thaysen et al., 2023). These studies have shown that significant trapping of the hydrogen is possible, which potentially limits the efficiency of storage and retrieval.

One feature of injection and withdrawal that has received less attention, however, is the potential rearrangement of the gas in the pore space, which is normally completely ignored for hydrocarbon production. However, a mechanism that could act to reconnect trapped gas is Ostwald ripening: differences in local capillary pressure of trapped ganglia result in differences in the gas pressure and consequently lead to concentration gradients in the aqueous phase thanks to small differences in solubility. Diffusion through the aqueous phase will equilibrate these gradients, leading to the growth of low-pressure bubbles and the shrinkage, if not complete disappearance, of ganglia with higher pressures. In a bulk fluid, the equilibrium state is the aggregation of all the gas in a single bubble; in porous media, multiple equilibrium states are possible with a distribution of ganglia of equal capillary pressure. This process has been explored in the context of carbon dioxide storage, experimentally, numerically and theoretically, and has also been observed for trapped air and natural gas (de Chalendar et al., 2018; Gao et al., 2022; Garing et al., 2017; Singh et al., 2022; Xu et al., 2017). However, hitherto no direct studies of Ostwald ripening (Ostwald, 1897) have been made for hydrogen, despite the likely rearrangement of gas over day-long time scales at the mm-scale thanks to hydrogen's high diffusion coefficient in water (Blunt, 2022).

To study trapping and Ostwald ripening, we have imaged hydrogen trapped inside a Bentheimer sandstone in situ via high-resolution X-ray tomography for drainage, and imbibition, representing injection and withdrawal, respectively. We also waited after displacement to observe how the fluids reconfigured in the pore space. Nitrogen, as a benchmark gas, with low solubility and relatively low diffusion coefficient in water, was also studied as a comparison.

## 2. Materials and Methods

A cylindrical Bentheimer sandstone sample (6.08 mm diameter and 28.76 mm length) was mounted in a specially designed micro-fluidics apparatus: details can be found elsewhere (Gao et al., 2017; Scanziani et al., 2018; Zhang, Bijeljic, & Blunt, 2022; Zhang, Lin et al., 2022). The sample and system were vacuumed for 10 hr and followed by injecting 200 pore volumes (PV) brine (distilled water with 3.4 wt% KI, potassium iodide) at 1 ml/min flow rate with 1 MPa back (fluid) pressure to reach a fully saturated condition. The temperature of the experiments was set at 25°C.

We conducted the investigations by the following steps.

1. Hydrogen injection (drainage) for 40 PV with a 0.04 ml/min injection rate; the capillary number was  $2.55 \times 10^{-9}$ .
2. Brine injection (imbibition) at the same flow rate and with the same pore volumes injected as in step 1; the capillary number was  $2.62 \times 10^{-7}$ .
3. 12 hr storage period. Here the system was left with no flow.

A ZEISS Xradia Versa 520 X-ray microscope was used to image the rock and fluids after each step with a 3.58  $\mu\text{m}$  voxel size: the settings were 75 kV X-ray energy, 0.5 s exposure time, and 1601 projections with a flat panel detector. The imaged volume was in the middle of the sample, with the field of view being  $1608 \times 1608 \times 2933$  voxels. After the hydrogen experiment, we injected many pore volumes of brine again to dissolve the hydrogen completely to reach an initial full brine saturation, and then we repeated the experiments as before but with nitrogen rather than hydrogen.

## 3. Results and Discussion

### 3.1. Phase Configurations in Drainage and Imbibition

The pore-scale X-ray images are shown in Figure 1: in the greyscale images, gas is black, brine is dark gray, and the rock is light gray; in the segmented images, the gas phase is yellow, brine is blue, and rock is gray. The results clearly show that after the gas drainage (Step 1), the nitrogen had the higher pore volume fraction (saturation);

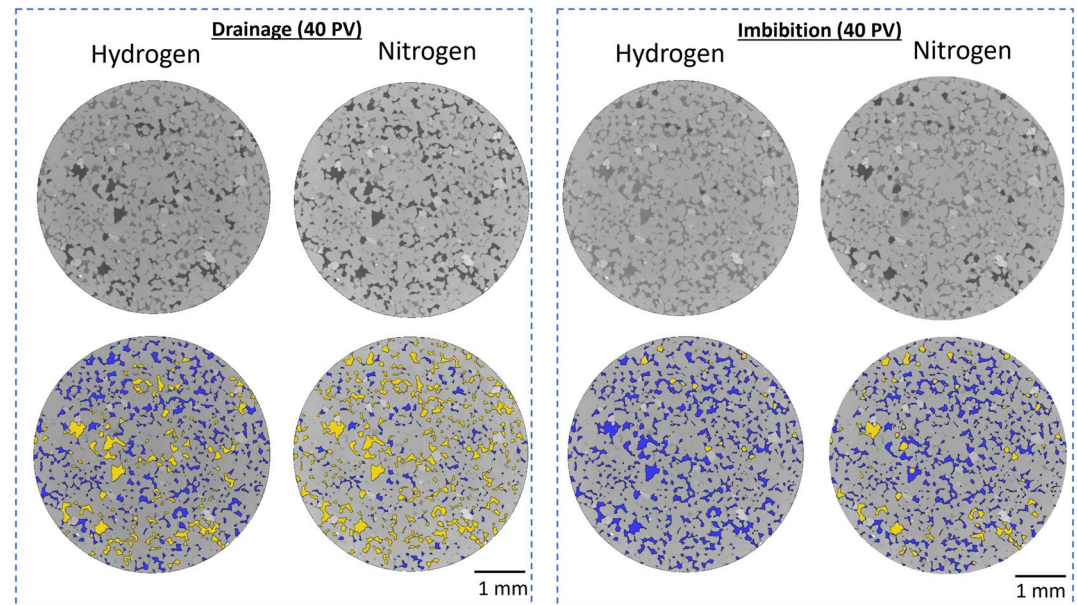


**Figure 1.** Example two-dimensional cross-sections of the three-dimensional images showing the same area of the sample after 40 pore volumes (PV) drainage and imbibition for hydrogen and nitrogen experiments. The greyscale images are shown at the top. In the segmented images below, yellow is gas, blue is water, and gray is rock matrix.

it is 0.83, almost twice that for hydrogen (0.44), quantified from the segmented images. The residual nitrogen saturation is 0.36 after imbibition (Step 2) but is only 0.11 in the hydrogen experiment. The lower hydrogen saturations can be explained by channeling through the pore space driven by the lower hydrogen viscosity of  $0.88 \times 10^{-5}$  Pa.s, compared to nitrogen,  $1.76 \times 10^{-5}$  Pa.s (Engineering ToolBox, 2014). In addition, during imbibition, a significant fraction of the hydrogen can dissolve in the injected brine.

### 3.2. Ganglia Size Distribution and Wettability

After the 12 hr storage period (Step 3), the X-ray images show a significant change in the hydrogen experiment but not in the nitrogen case: many small hydrogen ganglia that were trapped in Step 2, disappear, but larger bubbles grow, as illustrated in Figures 2 and 3. The discrete ganglia are identified, and their volume is quantified. Initially, the trapped ganglia of hydrogen are mainly located in the  $10^3$ – $10^4$   $\mu\text{m}^3$  range; however, it moves to larger sizes,  $10^6$ – $10^7$   $\mu\text{m}^3$ , after 12 hr. In contrast, there is little change in the distribution for nitrogen, with most volume in ganglia of size  $10^6$ – $10^7$   $\mu\text{m}^3$ , although there is a small shift toward larger ganglia. Note that the overall volume of gas does not significantly change—bubbles are not somehow removed from the system; instead, the size distribution changes while maintaining the same amount of gas in its own phase.

We also mapped the contact angle distributions between gas, brine and rock for all three steps in Figure 4, based on a subset of the whole image of size  $600 \times 600 \times 600$  voxels. The contact angles were obtained through an automated algorithm (AlRatrouf et al., 2017). In all cases, the contact angles are centered at  $60$ – $70^\circ$ , indicating weakly water-wet conditions, consistent with the quartz contact angle measurements of Iglauer et al. (2021). As expected from the lack of ganglion rearrangement in nitrogen, the contact angle distributions after all three steps are similar. However, we do observe an increase of around  $10^\circ$  in contact angle after waiting 12 hr for hydrogen. This is consistent with Ostwald ripening. Trapping initially occurs principally through snap-off in the tightest, most water-wet regions of the pore space. Smaller contact angles lead to larger interfacial curvature, higher local capillary pressures and greater solubility. The ganglia with locally smaller contact angles and higher capillary pressures then tend to lose gas volume in favor of larger ganglia with larger contact angles, lower interfacial curvature and lower solubility. This is illustrated in Figure 3, where the pores where water seems more wetting lose hydrogen in favor of other regions where the contact angle appears to be larger, where the capillary pressure is lower. A new position of equilibrium is reached with larger contact angles and ganglia. This trend is not seen for nitrogen, as initially, there is a lot of trapping anyway with larger ganglia present.

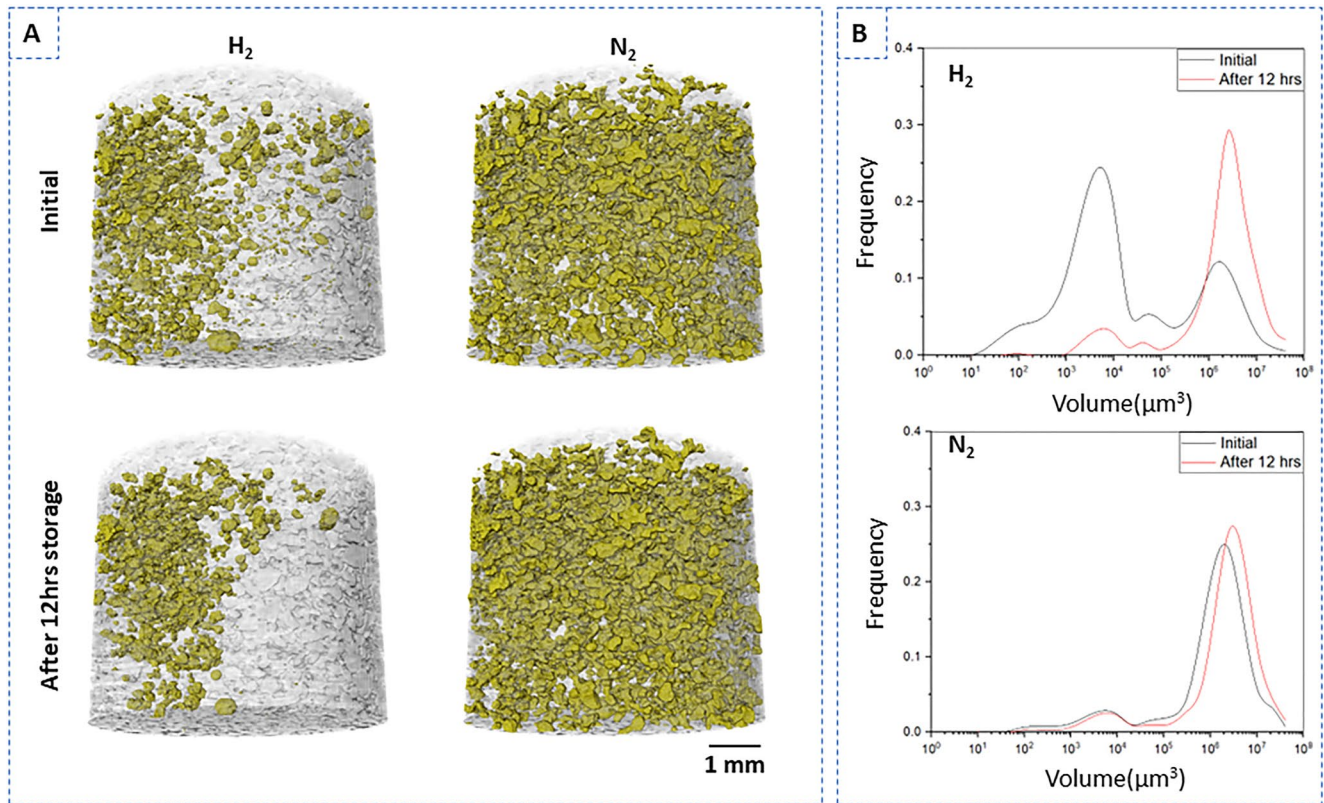


**Figure 2.** (a) 3D images of the trapped gas ganglia before and after 12 hr for both the hydrogen and nitrogen experiment: yellow represents trapped gas ganglia. (b) The quantified ganglia size distributions are shown with equal bin sizes in logarithmic space: this is equivalent to a volume-weighted distribution. The area under the distributions remains the same, indicating no change in gas volume.

We also assessed wettability through measuring interfacial area on the same subvolume; the results are shown in Table 1. For the hydrogen experiment we see a significant decrease in area between water and gas after 12 hr, consistent with the aggregation of smaller ganglia into larger ones. If the system is water-wet we expect the water to preferentially coat the solid surfaces. The ratio of the fraction of the solid contacted by the water to the saturation can be used as a measure of wettability: a value greater than 1 indicates a water-wet system, as seen here (Garfi et al., 2022). However, uncertainties in the measurement of interfacial area, and the low gas saturations, mean that we cannot determine any clear trends in wettability between the hydrogen and nitrogen experiments.

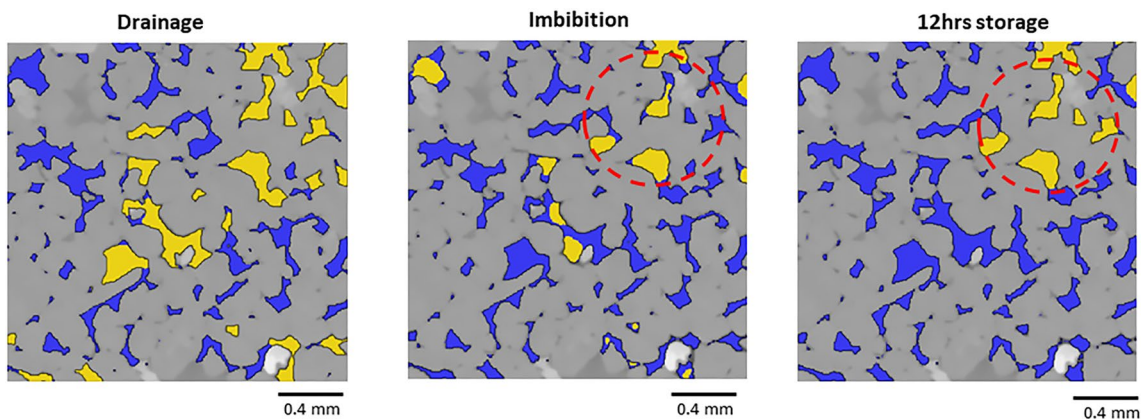


**Figure 3.** Examples of two-dimensional slices on a  $600 \times 600 \times 600$  voxel image for the hydrogen experiments after drainage, imbibition and after waiting a further 12 hr. Yellow is the hydrogen, blue is the brine, and gray is the rock. Note that some smaller ganglia, where water appears to be strongly wetting, disappear while other trapped regions grow, displacing brine. The red circle area is an example of where the hydrogen ganglia enlarged.

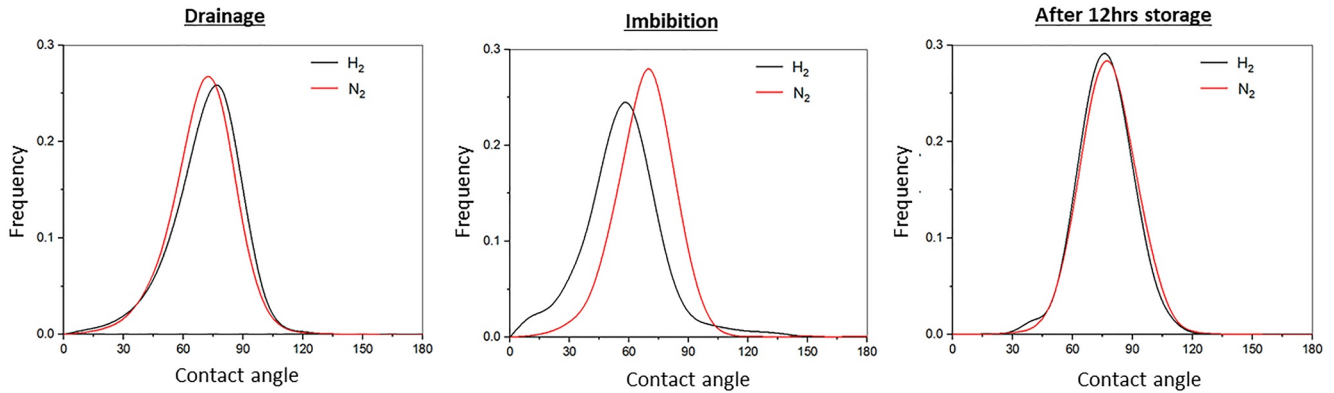


**Figure 4.** The distribution for contact angles between gas, brine and solid after drainage, imbibition and after waiting 12 hr for both nitrogen and hydrogen experiments.

### 3.3. Time-Scales for Ostwald Ripening

We will now estimate the time scale for Ostwald ripening to have a significant effect on the ganglion distribution, using Henry's, Fick's and the ideal gas laws, to show that this is possible for the hydrogen experiment. In a gas brine system, the equilibrium concentration of gas is the function of the pressure of gas,  $P_g$ , by Henry's law:

$$C = HP_g \quad (1)$$

where  $H$  is the Henry's Law constant. Concentration is defined in  $\text{mol.m}^{-3}$  and pressure in Pa. Therefore, typical concentration differences between ganglia can be approximated as,

$$\Delta C = H \Delta P = H \frac{\sigma}{r} \quad (2)$$

where we have assumed that pressure differences between ganglia are of order a typical capillary pressure, where  $\sigma$  is the interfacial tension and  $r$  is a typical radius of curvature of a gas-brine meniscus.

The diffusive flux  $F$  of dissolved gas in  $\text{mol.s}^{-1}$  can be described by Fick's law,

$$F = AD \frac{\Delta C}{L} \quad (3)$$

where  $A$  is a typical pore area,  $D$  is the diffusion coefficient of the gas in the aqueous phase, and  $L$  is the diffusion length.

We can then use this flux to estimate the time scale for a ganglion to completely disappear—as we see in the experiments.

**Table 1**

*Interfacial Areas, Saturation and the Ratio of Fractional Coverage to Saturation for the Experiments on  $600 \times 600 \times 600$  Voxels Cropped Image;  $a$  Is the Specific Interfacial Area (Area per Unit Volume),  $g$  Represents Gas (Nitrogen or Hydrogen),  $w$  Is Water and  $s$  Is Solid,  $S_w$  Is the Water Saturation*

Experiment	Nitrogen drainage	Nitrogen imbibition	Nitrogen imbibition after 12 hr	Hydrogen drainage	Hydrogen imbibition	Hydrogen imbibition after 12 hr
$S_w$	0.17	0.84	0.76	0.47	0.93	0.89
$a_{gw}$ [ $\text{mm}^{-1}$ ]	0.25	0.64	0.53	0.58	0.64	0.19
$a_{ws}$ [ $\text{mm}^{-1}$ ]	5.2	18.8	20.3	13.2	19.3	19.5
$a_{gs}$ [ $\text{mm}^{-1}$ ]	13.9	1.5	2.8	8.0	0.6	0.7
$f_w$	0.27	0.93	0.88	0.62	0.97	0.97
$f_w/S_w$	1.6	1.1	1.2	1.3	1.0	1.1

*Note.* The wetted fraction is defined as  $f_w = a_{ws}/(a_{gs} + a_{ws})$ . The ratio  $f_w/S_w$  is a measure of wettability. If this ratio is greater than 1 it represents water-wet conditions.

$$t = \frac{n}{F} = \frac{PV}{FRT} \quad (4)$$

where  $n$  is the number of moles of gas in the ganglion and we have used the ideal gas law where  $V$  is volume,  $T$  is temperature and  $R$  is the universal gas constant. We assume that all the material is lost through Ostwald ripening and ignore the possibility that the ganglia—when they become very small—may be able to advect through the pore space and merge with larger neighbors directly.

When combining Equations 1–4, the time for the small ganglia to disappear is estimated to be

$$t = \frac{LrPV}{ADH\sigma RT} \quad (5)$$

We assume that the length  $L = 2$  mm, since this is the length scale over which we see ganglion rearrangement, Figure 2. Equation 5 also contains three related pore-scale quantities:  $V$ ,  $A$  and  $r$ . We can estimate  $V$  as the typical volume of a single-pore ganglion that disappears: from Figure 2b, we can estimate this to be approximately  $5 \times 10^{-15} \text{ m}^3$  ( $5 \times 10^3 \text{ }\mu\text{m}^3$ ). If we assume that the ganglion is spherical, its radius  $r = 23 \text{ }\mu\text{m}$ , which is almost exactly the threshold throat radius in Bentheimer for displacement ( $24 \text{ }\mu\text{m}$ ; Blunt, 2017). The equivalent cross-sectional area  $A = \pi r^2$ . Then we rewrite Equation 5 in terms of a typical pore radius as:

$$t = \frac{Lr^2 P}{3DH\sigma RT} \quad (6)$$

For the hydrogen water system,  $H$  is  $7.8 \times 10^{-6} \text{ mol.m}^{-3}.\text{Pa}^{-1}$  (Linstrom & Mallard, 2014),  $D$  is  $5.13 \times 10^{-9} \text{ m}^2.\text{s}^{-1}$  (Hemme & Van Berk, 2018), and  $\sigma$  is  $7.29 \times 10^{-2} \text{ N.m}^{-1}$  (Chow et al., 2018). For nitrogen,  $H$  is  $6 \times 10^{-6} \text{ mol.m}^{-3}.\text{Pa}^{-1}$  (Linstrom & Mallard, 2014),  $D$  is  $2 \times 10^{-9} \text{ m}^2.\text{s}^{-1}$  (Cadogan et al., 2014), and  $\sigma$  is  $4.7 \times 10^{-2} \text{ N.m}^{-1}$  (Linstrom & Mallard, 2014). When we put these values in Equation 6, we find a time of 19,000 s or approximately 5 hr for hydrogen and 100,000 s or 28 hr for nitrogen. What this implies is that for our experiments conducted over 12 hr, we may indeed see a significant influence of Ostwald ripening for hydrogen over the scale of 2 mm, but with less effect for nitrogen. In addition, from Figure 2, there are virtually no single-pore ganglia of nitrogen initially anyway, so rearrangement can only occur for larger ganglia with even longer time-scales: some small changes are seen but are less significant than for hydrogen. At elevated temperatures and pressures, from Equation 6, the time-scales will be larger, but still of order days to weeks at typical subsurface storage conditions, and hence still shorter than the likely month-to-year cycles of injection and withdrawal. Note that this is an approximate calculation, but what we observe in the experiments is consistent with the theoretical analysis. Thus, we can conclude that, under the same conditions, nitrogen ganglia will take more than five times longer than hydrogen to disappear.

#### 4. Conclusions and Future Work

We imaged a sample of Bentheimer sandstone after drainage, imbibition and storage steps in both hydrogen–brine and nitrogen–brine systems. Due to channeling during initial injection and dissolution, less hydrogen was trapped in the pore space than nitrogen.

The main finding of this work was that after waiting 12 hr with no flow, we observed a significant rearrangement of trapped ganglia of hydrogen. Although the total mass of hydrogen stayed constant, smaller ganglia tended to disappear while larger ganglia grew. The average contact angle between hydrogen and brine also increased, as there was a tendency for the hydrogen to aggregate in less water-wet regions with a lower local capillary pressure. No noticeable change was seen for nitrogen.

We hypothesize that this rearrangement of ganglia is caused by Ostwald ripening: diffusion of dissolved gas in the aqueous phase in response to local concentration gradients, which drives the system to a state of equilibrium with constant local capillary pressure. This interpretation is consistent with other studies in the literature in 2D micromodels (Xu et al., 2017). We estimated the time scales for this to significantly change the fluid configuration over lengths of 2 mm: this was around 5 hr of hydrogen, consistent with the experiments.

The effect of Ostwald ripening is to equilibrate local capillary pressures and hence act to reduce capillary pressure hysteresis. While it may take many years for geological time scales to have a significant effect at the field

scale (Blunt, 2022), locally—at the mm to cm level—there is a significant rearrangement. This may then lead to a capillary pressure over a representative elementary volume that displays less hysteresis, indicating less trapping and more efficient injection and withdrawal, which is favorable for hydrogen storage and extraction.

Further work is thus required to test the hypothesis above, as well as studying the effect of the different temperature and pressure conditions. Experiments could be performed with higher initial gas saturations, perhaps imposed through a porous plate and at higher pressures, and with brine pre-equilibrated with gas to remove the complicating effect of dissolution. A careful analysis of repeated drainage and imbibition cycles with measurement, or estimation, of capillary pressure, could determine if indeed Ostwald ripening can lead to a less hysteretic capillary pressure than found in, for instance, oil-water systems where the ripening effect is negligible. This phenomenon would also affect relative permeability, meaning that the use of immiscible-type multiphase flow functions to model hydrogen storage, with quiescent periods of several months between injection and withdrawal, is flawed.

## Data Availability Statement

The data set in this paper can be accessed through Mendeley data: <https://doi.org/10.17632/rbkvwt7tws.1>.

## Acknowledgments

We thank Shell through the Digital Rocks programme for funding this work. We are grateful to Dr. Steffen Berg for suggesting that we study Ostwald ripening.

## References

- Aftab, A., Hassanpouryouzband, A., Xie, Q., Machuca, L. L., & Sarmadivaleh, M. (2022). Toward a fundamental understanding of geological hydrogen storage. *Industrial & Engineering Chemistry Research*, 61(9), 3233–3253. <https://doi.org/10.1021/acs.iecr.1c04380>
- Ali, M., Jha, N. K., Al-Yaseri, A., Zhang, Y., Iglauer, S., & Sarmadivaleh, M. (2021). Hydrogen wettability of quartz substrates exposed to organic acids; Implications for hydrogen geo-storage in sandstone reservoirs. *Journal of Petroleum Science and Engineering*, 207, 109081. <https://doi.org/10.1016/j.petrol.2021.109081>
- AlRatrou, A., Raeini, A. Q., Bijeljic, B., & Blunt, M. J. (2017). Automatic measurement of contact angle in pore-space images. *Advances in Water Resources*, 109, 158–169. <https://doi.org/10.1016/j.advwatres.2017.07.018>
- Blunt, M. J. (2017). *Multiphase flow in permeable media: A pore-scale perspective*. Cambridge University Press.
- Blunt, M. J. (2022). Ostwald ripening and gravitational equilibrium: Implications for long-term subsurface gas storage. *Physical Review E*, 106(4), 045103. <https://doi.org/10.1103/physreve.106.045103>
- Boon, M., & Hajibeygi, H. (2022). Experimental characterisation of H<sub>2</sub>/water multiphase flow in heterogeneous sandstone rock at the core scale relevant for underground hydrogen storage (UHS). *Scientific Reports*, 12(1), 1–12.
- Cadogan, S. P., Maitland, G. C., & Trusler, J. M. (2014). Diffusion coefficients of CO<sub>2</sub> and N<sub>2</sub> in water at temperatures between 298.15 K and 423.15 K at pressures up to 45 MPa. *Journal of Chemical & Engineering Data*, 59(2), 519–525. <https://doi.org/10.1021/je401008s>
- Chow, Y. F., Maitland, G. C., & Trusler, J. M. (2018). Interfacial tensions of (H<sub>2</sub>O + H<sub>2</sub>) and (H<sub>2</sub>O + CO<sub>2</sub> + H<sub>2</sub>) systems at temperatures of (298–448) K and pressures up to 45 MPa. *Fluid Phase Equilibria*, 475, 37–44. <https://doi.org/10.1016/j.fluid.2018.07.022>
- de Chalendar, J. A., Garing, C., & Benson, S. M. (2018). Pore-scale modelling of Ostwald ripening. *Journal of Fluid Mechanics*, 835, 363–392. <https://doi.org/10.1017/jfm.2017.720>
- Engineering ToolBox. (2014). Gases - dynamic viscosities.
- Gao, Y., Lin, Q., Bijeljic, B., & Blunt, M. J. (2017). X-ray microtomography of intermittency in multiphase flow at steady state using a differential imaging method. *Water Resources Research*, 53(12), 10274–10292. <https://doi.org/10.1002/2017wr021736>
- Gao, Y., Sorop, T., Brussee, N., van der Linde, H., Coorn, A., Appel, M., & Berg, S. (2022). Advanced digital-SCAL measurements of gas trapped in sandstone, paper SCA2022-043. In *Proceedings of SCA annual meeting*.
- Garfi, G., John, C. M., Rücker, M., Lin, Q., Spurin, C., Berg, S., & Krevor, S. (2022). Determination of the spatial distribution of wetting in the pore networks of rocks. *Journal of Colloid and Interface Science*, 613, 786–795. <https://doi.org/10.1016/j.jcis.2021.12.183>
- Garing, C., de Chalendar, J. A., Voltolini, M., Ajo-Franklin, J. B., & Benson, S. M. (2017). Pore-scale capillary pressure analysis using multi-scale X-ray microtomography. *Advances in Water Resources*, 104, 223–241. <https://doi.org/10.1016/j.advwatres.2017.04.006>
- Hashemi, L., Glerum, W., Farajzadeh, R., & Hajibeygi, H. (2021). Contact angle measurement for hydrogen/brine/sandstone system using captive-bubble method relevant for underground hydrogen storage. *Advances in Water Resources*, 154, 103964. <https://doi.org/10.1016/j.advwatres.2021.103964>
- Heinemann, N., Alcalde, J., Miocic, J. M., Hangx, S. J., Kallmeyer, J., Ostertag-Henning, C., et al. (2021). Enabling large-scale hydrogen storage in porous media—the scientific challenges. *Energy & Environmental Science*, 14(2), 853–864. <https://doi.org/10.1039/d0ee03536j>
- Hematpur, H., Abdollahi, R., Rostami, S., Haghighi, M., & Blunt, M. J. (2023). Review of underground hydrogen storage: Concepts and challenges. *Advances in Geo-Energy Research*, 7(2), 111–131. <https://doi.org/10.46690/ager.2023.02.05>
- Hemme, C., & Van Berk, W. (2018). Hydrogeochemical modeling to identify potential risks of underground hydrogen storage in depleted gas fields. *Applied Sciences*, 8(11), 2282. <https://doi.org/10.3390/app8112282>
- Iglauer, S., Ali, M., & Keshavarz, A. (2021). Hydrogen wettability of sandstone reservoirs: Implications for hydrogen geo-storage. *Geophysical Research Letters*, 48(3), e2020GL090814. <https://doi.org/10.1029/2020gl090814>
- Jangda, Z., Menke, H., Busch, A., Geiger, S., Bultreys, T., Lewis, H., & Singh, K. (2023). Pore-scale visualisation of hydrogen storage in a sandstone at subsurface pressure and temperature conditions: Trapping, dissolution and wettability. *Journal of Colloid and Interface Science*, 629, 316–325. <https://doi.org/10.1016/j.jcis.2022.09.082>
- Jha, N. K., Al-Yaseri, A., Ghasemi, M., Al-Bayati, D., Lebedev, M., & Sarmadivaleh, M. (2021). Pore scale investigation of hydrogen injection in sandstone via X-ray micro-tomography. *International Journal of Hydrogen Energy*, 46(70), 34822–34829. <https://doi.org/10.1016/j.ijhydene.2021.08.042>
- Linstrom, P. J., & Mallard, W. G. (2014). *NIST chemistry WebBook, NIST standard reference database number 69*. (p. 20899). National Institute of Standards and Technology.
- Miocic, J., Heinemann, N., Edlmann, K., Scafidi, J., Molaei, F., & Alcalde, J. (2022). Underground hydrogen storage: A review. *Geological Society, London, Special Publications*, 528(1), SP528–2022. <https://doi.org/10.1144/sp528-2022-88>

- Muhammed, N. S., Haq, B., Al Shehri, D., Al-Ahmed, A., Rahman, M. M., & Zaman, E. (2022). A review on underground hydrogen storage: Insight into geological sites, influencing factors and future outlook. *Energy Reports*, 8, 461–499. <https://doi.org/10.1016/j.egy.2021.12.002>
- Ostwald, W. (1897). Studien über die Bildung und Umwandlung fester Körper. *Zeitschrift für Physikalische Chemie*, 22(1), 289–330. <https://doi.org/10.1515/zpch-1897-2233>
- Parnell, J., & Blamey, N. (2017). Global hydrogen reservoirs in basement and basins. *Geochemical Transactions*, 18(1), 1–8. <https://doi.org/10.1186/s12932-017-0041-4>
- Raad, S. M. J., Leonenko, Y., & Hassanzadeh, H. (2022). Hydrogen storage in saline aquifers: Opportunities and challenges. *Renewable and Sustainable Energy Reviews*, 168, 112846. <https://doi.org/10.1016/j.rser.2022.112846>
- Scanziani, A., Singh, K., Bultreys, T., Bijeljic, B., & Blunt, M. J. (2018). In situ characterisation of immiscible three-phase flow at the pore scale for a water-wet carbonate rock. *Advances in Water Resources*, 121, 446–455. <https://doi.org/10.1016/j.advwatres.2018.09.010>
- Singh, D., Friis, H. A., Jettestuen, E., & Helland, J. O. (2022). A level set approach to Ostwald ripening of trapped gas bubbles in porous media. *Transport in Porous Media*, 145(2), 441–474. <https://doi.org/10.1007/s11242-022-01859-4>
- Thaysen, E. M., Butler, I. B., Hassanpouryouzband, A., Freitas, D., Alvarez-Borges, F., Krevor, S., et al. (2023). Pore-scale imaging of hydrogen displacement and trapping in porous media. *International Journal of Hydrogen Energy*, 48(8), 3091–3106. <https://doi.org/10.1016/j.ijhydene.2022.10.153>
- Xu, K., Bonnecaze, R., & Balhoff, M. (2017). Egalitarianism among bubbles in porous media: An Ostwald ripening derived anticoarsening phenomenon. *Physical Review Letters*, 119(26), 264502. <https://doi.org/10.1103/physrevlett.119.264502>
- Yekta, A. E., Manceau, J. C., Gaboreau, S., Pichavant, M., & Audigane, P. (2018). Determination of hydrogen–water relative permeability and capillary pressure in sandstone: Application to underground hydrogen injection in sedimentary formations. *Transport in Porous Media*, 122(2), 333–356. <https://doi.org/10.1007/s11242-018-1004-7>
- Zeng, L., Keshavarz, A., Xie, Q., & Iglauer, S. (2022). Hydrogen storage in Majiagou carbonate reservoir in China: Geochemical modelling on carbonate dissolution and hydrogen loss. *International Journal of Hydrogen Energy*, 47(59), 24861–24870. <https://doi.org/10.1016/j.ijhydene.2022.05.247>
- Zhang, Y., Bijeljic, B., & Blunt, M. J. (2022). Nonlinear multiphase flow in hydrophobic porous media. *Journal of Fluid Mechanics*, 934, R3. <https://doi.org/10.1017/jfm.2021.1148>
- Zhang, Y., Lin, Q., Raeini, A. Q., Onaka, Y., Iwama, H., Takabayashi, K., et al. (2022b). Pore-scale imaging of asphaltene deposition with permeability reduction and wettability alteration. *Fuel*, 316, 123202. <https://doi.org/10.1016/j.fuel.2022.123202>